Review of static and dynamic compressibility issues relating to deep underground salt caverns

Pierre Bérest, Jean Bergues, Benoît Brouard

Review of static and dynamic compressibility issues relating to deep underground salt caverns

P. Bérest, J. Bergues, B. Brouard*

Laboratoire de Mécanique des Solides, Centre commun X, Mines, Ponts, UMR 7649 CNRS, Ecole Polytechnique, 91128 Palaiseau, France

Compressibility of deep fluids-filled cavern is discussed. Compressibility is measured both through statical and dynamical tests. Statical compressibility is influenced by cavern shape and the nature of cavern fluids. This parameter plays an important role for such applications as the determination of stored hydrocarbons volume, of volume lost during a blow-out and of pressure build-up rate in a closed cavern. Dynamical compressibility is measured through the periods of waves triggered by pressure changes. Both tube waves and longer period waves associated to the existence of an interface between a liquid and a gas can be observed. They allow checking of the results of the statical tests and can provide additional information, for instance the existence of trapped gas in the well-head.

1. Introduction

In this paper we consider deep caverns (from 300 to 2000 m and more) that are connected to ground level through a cased and cemented well, which allows injection or withdrawal of fluids into or from the cavern (see Fig. 1).

These caverns are, in general, leached out from salt formations. The purpose of these caverns is to provide chemical plants with brine or, more commonly, to provide storage of large quantities of hydrocarbons. The volumes of such caverns range from 5000 to 1,000,000 m^3.

The mechanical behavior of such caverns is relatively complex, as rock salt rheology exhibits some unusual features. Many laboratory works have been devoted to it, but the subject hardly seems to be exhausted. Nevertheless, many authors [1–4] agree on several main features: the overall strain rate, $\dot{\varepsilon}$, of a sample submitted after time $t = 0$ to a constant load, σ, is the sum of elastic, steady-state and transient parts. The elastic part is described by a reversible and linear relation between $\dot{\varepsilon}$ and $\dot{\sigma}$ and the steady-state part by a constant strain rate reached after some days or weeks when a constant stress is applied. The transient part describes the rock behavior before steady-state is reached (Fig. 2). Many studies have focused on steady-state behavior, which is important for practical purposes. The main conclusions are as follows. Salt behaves like liquid, in the sense that it flows even under small deviatoric stresses. It is a non-Newtonian fluid and its steady-state strain rate is proportional to a rather high power ($n = 3$–6) of applied deviatoric stress. It is also strongly influenced by temperature.

The following expression for uniaxial steady-state creep is often adopted:

$$\dot{\varepsilon}^s = A \exp(-\mathscr{Q}/\mathscr{R}T_a)\sigma^n \tag{1}$$

where T_a is the absolute temperature (in K) and $\mathscr{Q}/\mathscr{R}$ ranges from 3000 to 10,000 K.

The general outline for the mechanical behavior of caverns is similar to that for a rock sample, but a clear understanding may require additional comments. One can distinguish among the following:

- Long-term steady-state creep is reached when the

* Corresponding author. Tel.: +33-1-69-333-343; fax: +33-1-69-333-026.

Nomenclature

$\tilde{a}$	acceleration (m s^{-2})
a,b	half axis of a spheroidal cavern (m)
A	constant for uniaxial steady-state creep (MPa^{-1} s^{-1})
B	parameter of steady-state creep law (MPa^{-n} s^{-1})
c	sound celerity (m/s)
c_a	sound celerity in air (m s^{-1})
c_b	sound celerity in brine (m s^{-1})
c_f	sound celerity in fluid (m s^{-1})
c_w	sound celerity in water (m s^{-1})
d	tube diameter (m)
e	a relative error (–)
E	Young's modulus (MPa)
f	cavern shape factor (–)
g	acceleration of gravity (m s^{-2})
G	average geothermal gradient (°C m^{-1})
h_1	gas column length at rest in the annular space (m)
h_2	gas column length at rest in the tube (m)
h_i	injected/saturated brines interface (m)
H	tube length (m)
H_i	brine/hydrocarbon interface (m)
K	parameter of transient creep law (MPa $day^{\alpha/\beta}$)
m	injected brine mass (kg)
M	cavern brine mass (kg)
n	exponent of the steady-state creep law (–)
P	absolute pressure (MPa)
P_{ann}	well-head annular space pressure (MPa)
P_c	cavern pressure (MPa)
P_{tub}	well-head tube pressure (MPa)
P_g	absolute gas pressure (MPa)
P_h	well-head hydrocarbon pressure (MPa)
P_R	lithostatic pressure at cavern depth (MPa)
P_1	absolute gas pressure at rest (MPa)
P_2	pressure at the bottom of a container (MPa)
Q	brine flow rate (m^3 s^{-1})
Q_{max}	maximum brine flow (m^3 s^{-1})
$\mathscr{Q}/\mathscr{R}$	parameter of steady-state creep law (K^{-1})
R	Reynolds number (–)
S	tube cross-section area (m^2)
$\tilde{S}$	annular cross-section area (m^2)
t	time (s)
T	oscillation period (s)
T_{min}	oscillation period in a brine-filled cavern (s)
T_a	absolute temperature (K)
u	brine speed (m s^{-1})
V	cavern volume (m^3)
V_{creep}	cavern volume loss by creep (m^3)
V_{inj}	brine injected volume (m^3)
V_{exp}	expelled volume during a blow-out (m^3)
x	hydrocarbon volume fraction (–)
α	thermal expansion coefficient ($°C^{-1}$)
β	compressibility factor (MPa^{-1})
β_b	brine compressibility factor (MPa^{-1})
β_b^{ad}	adiabatic brine compressibility factor (MPa^{-1})
β_c	cavern compressibility factor (MPa^{-1})
β_f^{ad}	fluid adiabatic compressibility factor (MPa^{-1})
β_h	Hydrocarbon compressibility factor (MPa^{-1})
β_{gas}^{isot}	Isothermal gas compressibility factor (MPa^{-1})
β_{prop}	Propane compressibility factor (MPa^{-1})
β_{sat}	Compressibility factor (slow evolution) (MPa^{-1})
β_t	Steel tube compressibility factor (MPa^{-1})
βV	Cavern compressibility (m^3 MPa^{-1})
$\delta\rho$	brine density difference (kg m^{-3})
$\Delta(.)$	any variation of a given quantity
ε	strain (–)
$\dot{\varepsilon}$	strain rate (s^{-1})
$\dot{\varepsilon}_s$	steady-state creep rate (s^{-1})
η	brine interface depth after a blow-out (m)
γ	gas adiabatic constant (–)
Γ	parameter of tube head losses law [$(m^3$ $s^{-1})^{-1.8}$]
κ	head losses parameter (Pa $s^{1.85}$ $m^{-2.85}$)
λ	dampening factor (s^{-1})
μ	tube brine mass (kg)
μ'	annular brine mass (kg)
ν	poisson's ratio (–)
ν_b	brine kinematic viscosity (m^2 s^{-1})
ρ_b	brine density (kg m^{-3})
ρ_f	fluid density (kg m^{-3})
ρ_h	hydrocarbon density (kg m^{-3})
ρ_{salt}	salt density (kg m^{-3})
ρ_{sat}	saturated brine density (kg m^{-3})
σ	stress (Mpa)
Σ	container cross-section (m^2)
τ	time (s)
χ	brine concentration (–)
χ^s	saturated brine concentration (–)
ω_o	pulsation (s^{-1})
$\bar{\omega}$	head losses (Pa m^{-1})
ω_1	pulsation in the annular space (s^{-1})
ω_2	pulsation in the tube (s^{-1})

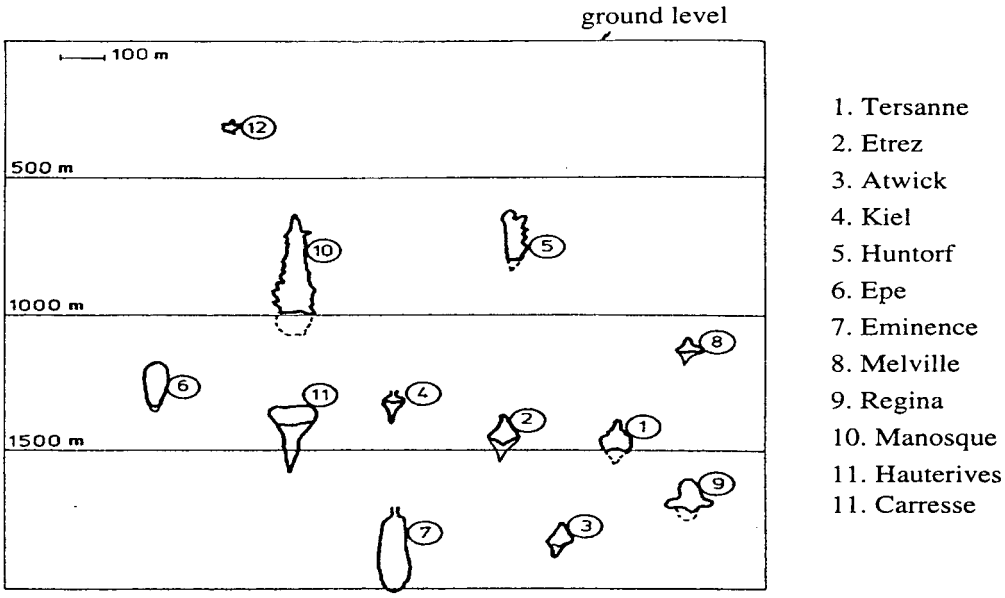

Fig. 1. Vertical cross-sections of several salt caverns.

cavern fluid pressure is kept constant for months or years. A typical value of relative cavern volume change rate due to steady-state creep for a 1000 m deep cavern submitted to *halmostatic* pressure (or the pressure of a cavern when the well is filled with saturated brine up to ground level, where it is opened to atmosphere — i.e. 12 MPa) is 3 10^{-4} per year. This value should be multiplied by 100 when the cavern is 2000 m deep (The *halmostatic* pressure equals 24 MPa.), because of the increases in both lithostatic pressure and temperature. In any case, these features are subject to large variations when different sites and cavern shapes are considered.

- Transient creep is triggered by any significant and rapid cavern pressure change. Its effect on the relative volume change rate can be one or two orders of magnitude larger than the steady-state value at the same average pressure level, but it is significant for only a few weeks (see, for instance, Hugout [5]). The transient creep effects in a cavern, even if very significant, are difficult to assess, for they combine with the effects of the additional salt dissolution or brine recrystallization which, as transient creep, follow any cavern pressure change (Ehgartner and Linn [6][1]). The "true" transient creep must be distinguished from the effect of steady-state creep changes that lead to a transient redistribution of the non-uniform stress field around the cavern, slowly moving from its initial to final distribution. This transient evolution can be several years long.
- Elastic behavior of the cavern, or cavern shape and volume changes, immediately follow any cavern pressure change. (As will be seen later, "immediately" requires definition.)

This last aspect has not yet been given much attention in the literature when compared to creep, which is of primary importance for cavern structural stability and life-long duration. Nevertheless, the elastic behavior of a cavern — more precisely, cavern compressibility — plays a very significant role in various phenomena, including mechanical-integrity test design (Bérest et al. [7]), pressure build-up rate in a closed cavern and blow-out scenarios (discussed later), among others. Useful information on cavern volume, the existence of trapped gas pockets and evaluation of the amount of hydrocarbon stored can be inferred from such measurement.

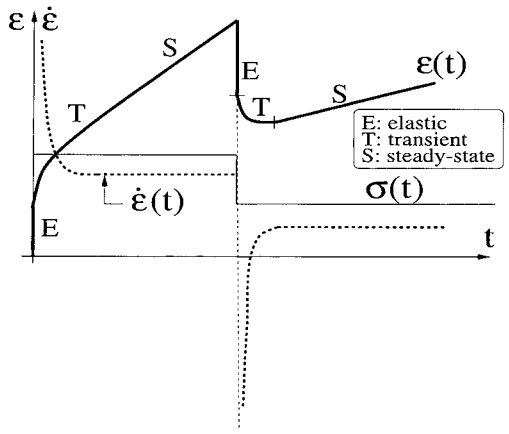

Fig. 2. Schematic stress-time/strain-time curves.

[1] The SMRI papers referenced below are available through the Solution Mining Research Institute 3336 Lone Hill Lane, Encinitas, California 92024, USA.

As for the mechanical behavior of any elastic body, cavern compressibility is apparent both through static and dynamic tests (i.e. involving waves triggered by a rapid change of pressure). These two aspects will be discussed successively.

Furthermore, it must be kept in mind that changes in cavern volume or shape cannot be directly observed; they are measured through experiments that involve flow and/or pressure measurements at the well-head. Brine (or, in general, stored fluids) properties and mass transfer from salt mass to brine influence the measurements results and must be taken into account, together with the mechanical properties of salt, for a thorough interpretation of the tests.

2. Static behavior

2.1. Cavern compressibility and the compressibility factor

When a certain amount of liquid, ΔV_{inj}, is injected in a closed cavern, the well-head pressure increases by ΔP which is also, at first approximation (see Section 2.5.1) the cavern pressure increase ΔP_c (Fig. 3). The relation between the two quantities is, in general, linear during a rapid test. A similar test can be performed by *withdrawing* a certain amount of liquid from a pressurized cavern.

An example is provided by a test described in Thiel [8] (Fig. 4). The slope of the curve (brine pressure versus injected brine) is called the *cavern compressibility* (in m^3/MPa or bbls/psi):

$$\Delta V_{\text{inj}} = \beta V \Delta P \tag{2}$$

To what extent the cavern compressibility, βV, is influenced by test duration and other factors will be discussed later; Fig. 4 proves that, from an engineer's point of view, the notion of cavern compressibility is defined sufficiently.

As a matter of fact, cavern compressibility, βV, can be expressed as the product of the cavern volume, V (in m^3) and a *compressibility factor*, β (in MPa^{-1}, or psi^{-1}). The compressibility factor, β, is a constant — at least for caverns of similar shapes located in the same site, filled with the same fluid and tested during a relatively short period (one hour); in other words, β is not dependent upon the *size* of the cavern.

For instance, for the Etrez and Tersanne natural gas storage sites, operated by Gaz de France in the north of Lyon (France), Boucly [9] has measured the compressibility factor:

$$\beta = 4.0 \times 10^{-4}\ \text{MPa}^{-1} = 2.8 \times 10^{-6}\ \text{psi}^{-1} \tag{3}$$

which must be considered as an average value. (Smaller values, from 3.4×10^{-4} to 3.9×10^{-4} MPa^{-1}, have been found in Tersanne caverns.)

Similarly, for the case of the Manosque oil storage site operated by Geostock in southeastern France, Colin and You [10] give the measured compressibility factor for brine-filled caverns:

$$\beta = 5.0 \times 10^{-4}\ \text{MPa}^{-1} = 3.4 \times 10^{-6}\ \text{psi}^{-1} \tag{4}$$

For the caverns of the Vauvert site operated by ELF in southeastern France, You et al. [11] have measured values scattered between $\beta = 3.2 \times 10^{-4}$ to 8.5×10^{-4} MPa^{-1}, which does not seem consistent with the statement of constant β for a given site. In this particular case, however, (i) the caverns are very deep, resulting in large creep rates, (ii) the salt formation is probably gassy and (iii) caverns develop between two wells

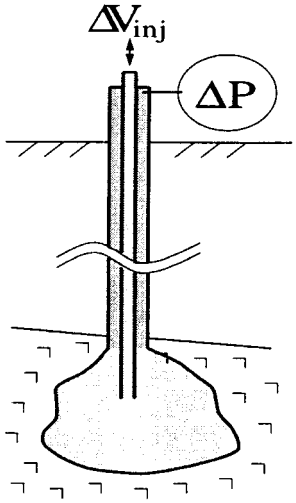

Fig. 3. Measurement of cavern compressibility.

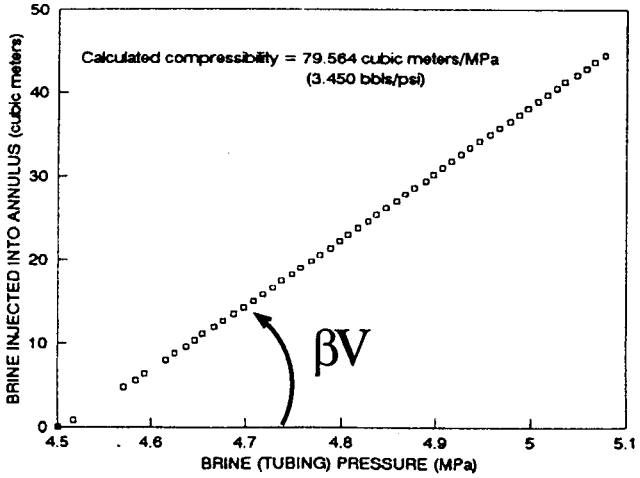

Fig. 4. Prepressurization of a domal cavern (Thiel [8]).

linked by hydrofrac. These factors can contribute to this unusual scattering.

2.2. The compressibility factor

We first consider the case of a brine-filled cavern and will restrain in this paragraph to simple derivation; difficulties will be dealt with later. Let M be the cavern brine mass:

$$M = \rho_b V \tag{5}$$

where ρ_b is the brine density, and V is the cavern volume.

When the cavern pressure rapidly increases by ΔP_c (by "rapidly" we mean that neither salt creep nor salt dissolution are afforded enough time to play a significant role; Section 2.5.3), the following occurs:

1. The brine density increases by $\Delta\rho_b = \rho_b \beta_b^{ad} \Delta P_c$, where β_b^{ad} is the brine adiabatic compressibility factor. It does not depend upon cavern shape or cavern volume.
2. The cavern volume increases by $\Delta V = \beta_c \Delta P_c V$, where β_c is the cavern compressibility factor, which depends upon rock-mass elastic properties and cavern shape (but *not* upon cavern volume).

Then, if an additional mass of saturated brine, $m = \rho_b \Delta V_{inj}$, is forced into a closed cavern, its pressure will increase by

$$M + m = (\rho_b + \Delta\rho_b)(V + \Delta V) \tag{6}$$

or after linearization

$$\beta V \Delta P_c = \Delta V_{inj}; \quad \beta \approx \beta_b + \beta_c \tag{7}$$

The compressibility factor, β, is the sum of the brine compressibility factor, β_b, and the cavern compressibility factor, β_c.

2.3. The cavern compressibility factor

The cavern compressibility factor, β_c, obviously depends upon both rock-salt elastic properties and cavern shape.

2.3.1. Theoretical analysis

For simple cavern shapes, some analytical calculations can be made. If E is the Young's modulus of the salt and ν is its Poisson's ratio, we get the following:

Cavity shape	Sphere	Infinite cylinder	Real-world
β_c	$[3(1+\nu)/2E]$	$[2(1+\nu)/2E]$	$f(\nu) \times (1+\nu)/E$

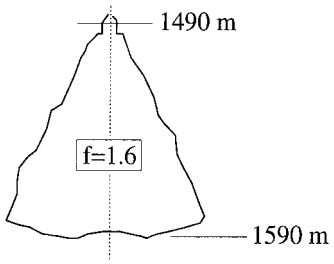

Fig. 5. Tersanne Te04 cavity (Gaz de France).

where $f = f(\nu)$ is a shape factor that depends on the cavern's shape and, to a smaller extent, on the Poisson's ratio of the rock; and f is always greater than 3/2, which corresponds to the spherical case, which is the less compressible shape of a cavern. In the case of the Te04 cavern (Fig. 5), Gaz de France computed a $f = 1.6$ shape factor.

It is interesting to consider the case of a spheroidal cavern (obtained by rotation of an ellipse around its vertical axis; Fig. 6) for which a closed-form solution is available. Let us define the aspect ratio as b/a. A prolate spheroidal cavern (b/a is large) behaves as a cylindrical cavern ($\beta_c \approx 2(1+\nu)/E$): when $b = a$, we get the spherical case; when the cavern becomes oblate (flat) or when a/b is large, the cavern compressibility factor drastically increases, $\beta_c \approx (4(1-\nu)^2/E\pi)(a/b)$ and the cavern compressibility is $\beta V \approx \beta_c V = (16/3) \times (1-\nu)^2/E)a^3$ (Fig. 6), Patrick Ballard, Andrei Constantinescu (personal communication).

2.3.2. Field data

From compressibility factor data, Boucly [9] infers that $\beta_c = 1.3 \times 10^{-4}\text{MPa}^{-1}$ (9.0×10^{-7} psi^{-1}), which is consistent, for instance, with the following estimates:

$$\nu = 0.3 \quad E = 17{,}000 \text{ MPa} \quad f = 1.7 \tag{8}$$

This shape-factor value corresponds to caverns from

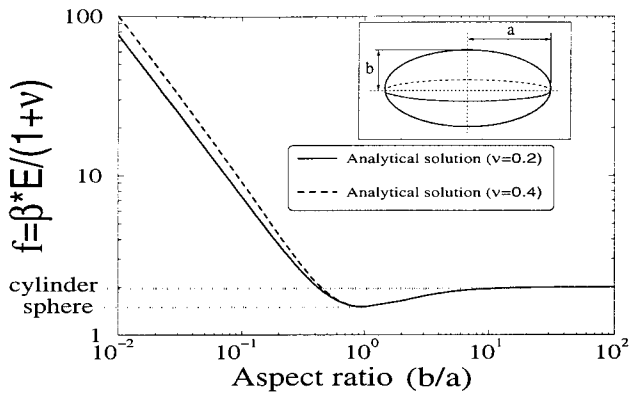

Fig. 6. Cavern compressibility factor for a spheroidal cavern.

$$\begin{cases} \Delta V = \beta_c V \Delta P + \Delta V_{creep} + \dfrac{\rho_b V}{(1-\chi)\rho_{salt}} \dfrac{d\chi^s}{dP} \Delta P \\ \Delta V_{inj} \left[\beta_c + \beta_b^{ad} + \left(\dfrac{1}{\rho_b} \dfrac{\partial \rho_b}{\partial \chi} - \dfrac{(\rho_{salt} - \rho_b)}{(1-\chi)\rho_{salt}} \right) \dfrac{d\chi^s}{dP} \right] V \Delta P + \Delta V_{creep} = \beta^{sat} V \Delta P + \Delta V_{creep} \end{cases} \quad (10)$$

the Tersanne and Etrez sites whose shapes are intermediate between cylindrical and spherical (Fig. 5). The elastic properties of rock salt can vary from one site to another; reasonable ranges of variation are

$$\begin{cases} 5000 \leq & E \leq & 40{,}000 \text{ MPa} \\ 0.25 \leq & \nu \leq & 0.3 \end{cases} \quad (9)$$

With such figures, the cavern compressibility factor can vary from $\beta_c = 0.5 \times 10^{-4}$ MPa^{-1} to $\beta_c = 4 \times 10^{-4}$ MPa^{-1} for a spherical cavern (the less compressible shape) and up to 4 or 5 times more for a somewhat flat cavern.

2.4. The fluid compressibility factor

2.4.1. Brine

The theoretical adiabatic brine-compressibility factor is related to the sound of speed through the relation $\rho_b \beta_b^{ad} c_b^2 = 1$, where $\rho_b = 1200$ kg m^{-3}, $c_b = 1800$ m s^{-1}; thus, $\beta_b^{ad} \approx 2.57 \times 10^{-4}$ MPa^{-1}. This figure suits rapid (adiabatic) evolutions; β_b^{ad} is not different, from a practical point of view, from the brine isothermal compressibility factor, but it is a little too small when relatively slow pressure changes (several hours or days long) are considered, because the brine saturation concentration is modified by pressure change. Pressure build-up triggers additional cavern leaching, (as noted, for instance, by Ehgartner and Linn [6]) and increases the cavern volume, resulting in a slightly higher effective brine compressibility factor. Brine density is a function of pressure and salt concentration, $\rho_b = \rho_b(P,\chi)$ in turn, at saturation, concentration is a function of pressure (Temperature is assumed to be constant.), or $\chi^s = \chi^s(P)$. Then cavern volume change (ΔV) is the sum of the elastic change (as seen above), of the volume change due to transient and steady-state creep (ΔV_{creep}, positive when the cavern enlarges) — at least when very long term evolutions are considered, as in Section 2.6.2 — and of the volume increase due to salt dissolution.

On the other hand, when evaluating the average brine density — i.e. the ratio between the cavern brine mass and the cavern volume — both the influence of the brine concentration on brine density and the mass change due to salt dissolution must now be taken into account.

When writing water and salt balances during a pressure change, one gets the following expressions (Brouard [12])

where ρ_{salt} is salt density ($\rho_{salt} \approx 2200$ kg m^{-3}) and β^{sat} is the compressibility factor during a slow enough test for the brine being saturated at any instant or

$$\Delta V_{inj} = \beta^{sat} V \Delta P \approx (\beta_c + 1.06 \beta_b^{ad}) V \Delta P \quad (11)$$

(when creep is neglected) which means that the compressibility factor β^{sat} during a slow test is larger by approximately 4% than its instantaneous ("adiabatic") counterpart $\beta = \beta_c + \beta_b^{ad}$ ($\beta_c \approx 1.3 \times 10^{-4}$ MPa^{-1}).

This additional compressibility is not immediately effective, because salt dissolved at a cavern wall must be transported through convection and diffusion until chemical equilibrium in the whole brine body is restored. Kinetics are difficult to assess and impossible to measure in situ, as dissolution effects and transient creep effects are interlocked.

As a conclusion, a reasonable value for the in-situ brine compressibility factor seems to be $\beta_b = 2.7 \times 10^{-4}$ MPa^{-1} (1.9×10^{-6} psi^{-1}), Boucly [9] or Crotogino [13], but it must be kept in mind that this value can be influenced by test duration.

2.4.2. Hydrocarbons

Hydrocarbons are much more compressible than brine or water. Their compressibility factors are influenced by pressure and temperature. A typical value for pure propane at 25°C and 7 MPa is $\beta_{prop} \approx 2.9 \times 10^{-3}$ MPa^{-1}; it is slightly higher (up to 4.5×10^{-3} MPa^{-1}) for industrial propane.

2.4.3. Nitrogen and other gases

As long as only slow (more than one hour for a gas volume of a few cubic meters) evolutions are considered, gas evolutions can be considered to be isothermal; for an ideal gas, the compressibility factor is simply the inverse of the (absolute) pressure, P:

$$\beta_{gas}^{isot} = 1/P \quad (12)$$

This means that the compressibility factor of a gas pocket trapped at the top of a brine-filled cavern (where the pressure is, for instance, $P_c = 12$ MPa at 1000 m), will be

$$\beta_{gas}^{isot} \approx 8.3 \times 10^{-2} \text{ MPa}^{-1} \quad (13)$$

and the compressibility factor of a gas bubble trapped at the well-head, where the absolute pressure is, for

instance, 0.1 MPa, will be

$$\beta_{\text{gas}}^{\text{isot}} = 10\ \text{MPa}^{-1} \tag{14}$$

For other gases, the inverse of absolute pressure provides a first estimation of the compressibility, which can be refined by consulting available physical constant tables.

2.4.4. The case of several fluids in a cavern

- Theoretical aspects

  In a storage cavern, the cavity contains brine *and* another fluid (such as propane or oil). In this case, the global fluid-compressibility factor will be a certain average of the compressibility factors of the different fluids: β_{b} (for brine) and β_{h} (for hydrocarbon). Let x be the cavern volume fraction that is occupied by the other fluid (i.e. if V is the cavern volume, the hydrocarbon volume is xV and the brine volume is $(1-x)V$). Then, the global compressibility factor β will be

$$\beta = \beta_{\text{c}} + (1-x)\beta_{\text{b}} + x\beta_{\text{h}} \tag{15}$$

This will vary, to a large extent, with respect to the hydrocarbon volume fraction. Consider, for instance, the case of propane storage. If we take

$$\begin{cases} \beta_{\text{c}} = 1.3 \times 10^{-4}\ \text{MPa}^{-1} \\ \beta_{\text{b}} = 2.7 \times 10^{-4}\ \text{MPa}^{-1} \\ \beta_{\text{h}} = \beta_{\text{prop}} = 4.5 \times 10^{-3}\ \text{MPa}^{-1} \end{cases} \Longrightarrow \beta$$

$$= 4 \times 10^{-4} + 42.3 \times 10^{-4} x \quad (\text{MPa}^{-1}) \tag{16}$$

the compressibility factor varies from $\beta = 4 \times 10^{-4}\ \text{MPa}^{-1}$ (no propane in the cavern) to $\beta = 38 \times 10^{-4}\ \text{MPa}^{-1}$ (propane fills 80% of the cavern).

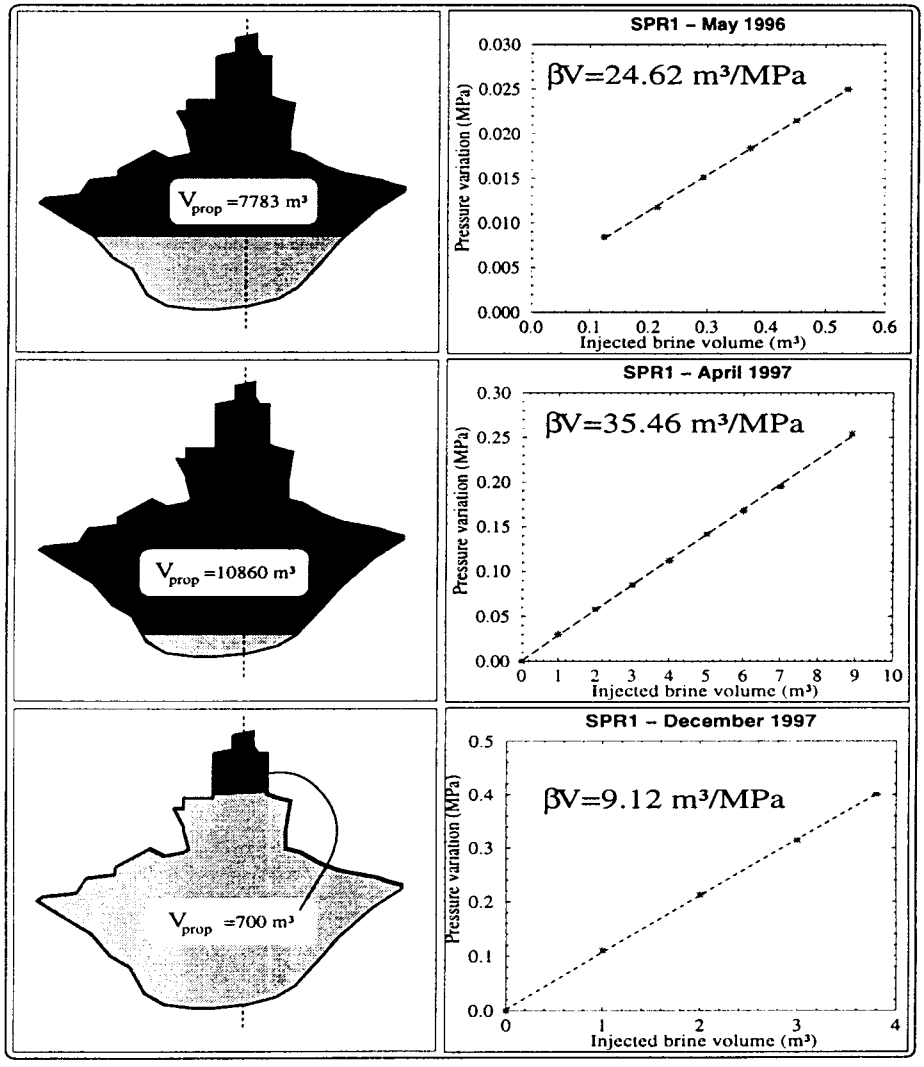

Fig. 7. Three cavern compressibility measurements on the Carresse SPR1 cavern.

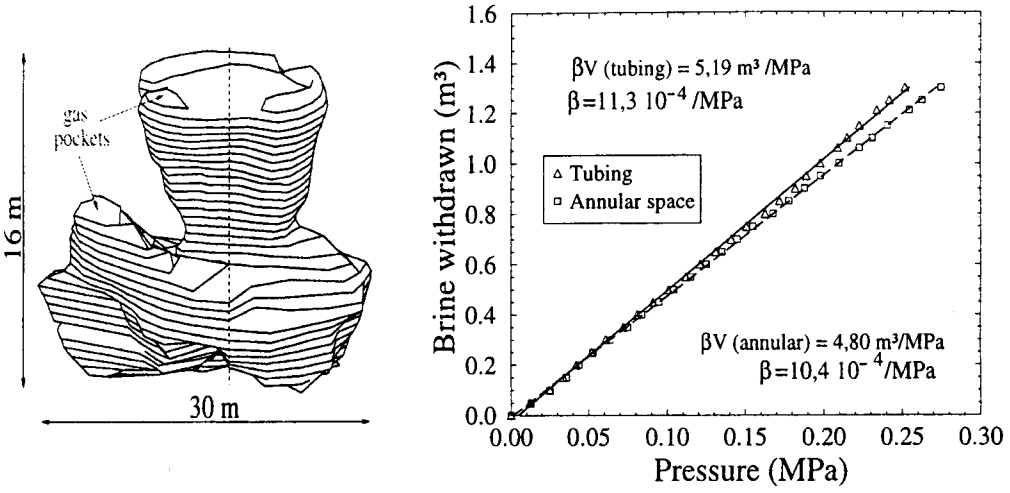

Fig. 8. A compressibility test on the Carresse SPR3 cavern.

- Example

  The SPR1 cavern in the Carresse site (in south-western France) is used by the SNEA(P) (ELF) company to store propane. The casing shoe depth is 348 m below ground level; the cavern bottom depth is 381.5 m. This cavern volume is 13,000 m^3 (as measured in 1992). We have performed compressibility factor measurements at three different periods (Fig. 7). During these three tests, the cavern compressibility (βV) was measured during a brine injection; the pressure measurement resolution was 500 Pa. This allows the propane volume in the cavern to be back-calculated. The computed propane volumes were compared with the operator's data obtained through surface flow-meters. The agreement with the above stated formula (15) is satisfactory if not perfect (in this case, propane compressibility factor is probably smaller than the theoretical figure given above). The reason may be that a definite testing protocol was not yet clearly set during the first tests.

2.4.5. The case of a gas pocket in a cavern

If a gas pocket is trapped in a cavern, the compressibility factor drastically increases, even if the pocket volume is small.

The SPR3 cavern of the SNEA(P) Carresse site is deeper than SPR1; the casing-shoe depth is 692 m below ground level and the cavern bottom depth is 711 m. The cavern volume is $V \approx 4600$ m^3. A 1995 sonar survey performed a few months before the test confirmed that this cavern exhibits a non-convex shape (Fig. 8). The compressibility factor observed during the test was $\beta \approx 11 \times 10^{-4}$ MPa^{-1}, which appears abnormally high for a brine-filled cavern (pressure resolution was 500 Pa). It soon appeared that this high figure could be explained by the presence of gas, coming from the salt formation or from the brine used for cavern leaching, which was trapped in gas pockets under the bell-shaped parts of the cavern. These pockets are clearly visible on the left and top of the cavern shown on Fig. 8. The gas pressure at cavern depth is $P_c = 8.3$ MPa, which means that its isothermal compressibility factor is $\beta_{gas}^{isot} = 0.12$ MPa^{-1}. The volume of the gas pocket can be back-calculated: it is approximately 25 m^3, or $x = 0.5\%$ of the cavern volume.

2.5. Phenomena influencing the measurement of cavern compressibility

2.5.1. Column weight changes

We assume here that brine is injected (or withdrawn) in (or from) the central tube, whose section is S; we compare the cavern well-head pressure as measured in the annular space (P_{ann}) and in the central tube, (P_{tub}). The pressure variation, ΔP_{ann}, in the annular space during an injection (or withdrawal) test is very close to the pressure variation, ΔP_c, in the cavern, because the composition, temperature and concentration of the fluid column in the annular space do not change

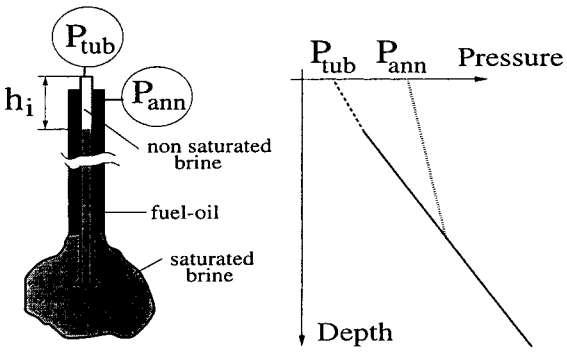

Fig. 9. Injection of non-saturated brine in the central tube.

during the test; only a very small difference due to brine compressibility can be observed. The same cannot be said of the brine column in the tube space (Fig. 9). In many cases, the injected brine is not fully saturated (because, for example, it is stored at ground level and can be lightened by rain water), resulting in significant variations of the brine column weight.

We assume that the density of the injected brine is slightly smaller than the density of saturated brine (temperature effect will be dealt with later), for instance, $\rho_b = 1180$ kg m^{-3} instead of $\rho_{sat} = 1200$ kg m^{-3}, which results in a ($\delta\rho = 20$ kg m^{-3}) gap in densities. This means that when a volume of brine equal to ΔV_{inj} is injected in the cavern, the injected-brine/saturated-brine interface is lowered by $h_i = \Delta V_{inj}/S$ and the cavern pressure (and annular space pressure) change by

$$\Delta P_{ann} = \Delta P_c = \frac{\Delta V_{inj}}{\beta V} = \frac{S h_i}{\beta V} \tag{17}$$

The tube pressure, however, changes by

$$\Delta P_{tub} = \Delta P_c + \delta\rho g h_i \tag{18}$$

due to change in the brine column weight (now the tube column contains some unsaturated brine).

In other words, provided that the injected brine volume, ΔV_{inj}, is smaller than the tube volume, we get a relative error, e, when measuring the tube pressure:

$$e = \frac{\Delta P_{tub} - \Delta P_{ann}}{\Delta P_{ann}} = \frac{\beta V g \delta\rho}{S} \tag{19}$$

Thus, reasonable values are $g = 10$ m s^{-2}, $S = 2 \times 10^{-2}$ m^2. For a brine-filled cavern, $\beta = 4 \times 10^{-4}$ MPa^{-1}; then, e, the relative error made by measuring the tube brine pressure instead of annular brine pressure, is a function of cavern volume (V) and brine distance to saturation ($\delta\rho$):

$$e = 2 \times 10^{-7} V \quad (\text{in m}^3)\ \delta\rho \quad (\text{in kg/m}^3) \tag{20}$$

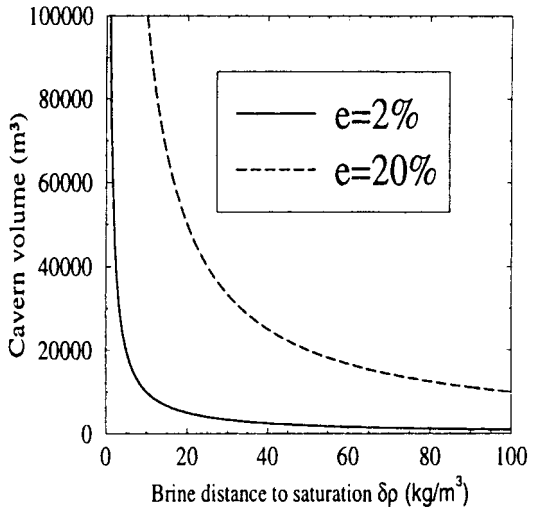

Fig. 10. Iso-underestimations of the cavern compressibility βV when injecting undersaturated brine.

Large under-estimations of cavern compressibility can be made by measuring the pressure variations on the wrong tube (Fig. 10). They can be avoided by either (i) measuring the well-head pressure variations in the annular space, or (ii) pressurizing the cavern and performing a test by withdrawing (instead of injecting) brine. (Note, however, that transient creep effects can be a drawback; Section 2.5.3).

It must be noted that a similar effect can be reached when a volume $\Delta V_{inj} = S h_i$, $h_i < H$, where H is the well length, is so rapidly injected or withdrawn in or from the well that thermal equilibrium with the rock mass is not reached during the test. For instance if brine is withdrawn, the average well temperature will increase by $\Delta T_a = h_i(1 - h_i/2H)G$, where G is the average geothermal gradient ($G = 3 \times 10^{-2}$ °C m^{-1} is typical, but smaller values must be expected in salt formations.), resulting in a density change $\delta\rho = \alpha\rho_b G h_i$, where the thermal expansion coefficient of brine is $\alpha = 4.4 \times 10^{-4}$ °C^{-1}. In this case, for $h_i = 500$ m, $H = 1000$ m, we have $\delta\rho = 6$ kg m^{-3}, leading to large over-estimations, at least in large caverns.

2.5.2. Brine heating and percolation

Because of brine heating, an opened cavern expels brine (or pressure builds up in a closed cavern (Bérest and Brouard [14]). This effect is most significant when the cavern has been recently leached; a typical value is 200 l day^{-1} for a 8000 m^3 cavern (Hugout [5]). This figure is proportional to the cubic root of the cavern volume; for instance, the rate would be 800 l day^{-1} in a 500,000 m^3 cavern. This means that injection test results will be seriously affected if the injection rate is smaller than, say, 1 m^3 h^{-1}. In many cases, the injection rate is faster and brine heating is not a serious concern. The same can be said of steady-state creep (transient creep will be discussed in Section 2.5.3), except for very deep caverns (2000 m below ground level). Finally, brine percolation, which is a real concern for tests performed in pressurized wells before leaching, does not seem to have a large influence (Bérest et al. [7]), except perhaps in some very specific cases. An example is described in Istvan et al. [15].

2.5.3. Transient creep

Steady-state creep is, in most cases, negligible: it is too slow to bring significant perturbations during a pressurization or depressurization test, except for the possible case of a very deep cavern (2000 m below ground level).

However, a rapid change of pressure as it can exist

at the beginning of a compressibility test triggers transient creep that can be of bigger concern from the perspective of test accuracy. According to Dubois and Clerc-Renaud [16], who describe such tests performed in the Manosque facility (France), this effect seems to be more pronounced during depressurization. From a practical point of view, it is difficult to separate this transient creep effect from the effects of additional salt dissolution.

In order to simulate such a phenomenon, we have used the constitutive law proposed by Gaz de France (Hugout [5]) which takes into account transient creep and whose uniaxial formulation is

$$\dot{\varepsilon} = 10^{-6}\frac{\sigma^{\beta-1}}{K^{\beta}}\frac{\mathrm{d}}{\mathrm{d}t}\int_{-\infty}^{t}\frac{\mathrm{d}\sigma}{\mathrm{d}\tau}(t-\tau)^{\alpha}\mathrm{d}\tau \tag{21}$$

(of course, the α and β exponents have not the same sense here as before).

We made calculations for the case of a 100,000 m^3 cavern at a depth of 1000 m; with $K = 0.85$ MPa day$^{\alpha/\beta}$, $\alpha = 0.36$, $\beta = 3$, the pressure rate for this case was 1 MPa/h (Fig. 11). In this case, transient creep effect is significant after an hour or two.

2.6. Applications

2.6.1. Volume of fluid lost during a blow-out

Van Fossan and Whelpy [17] remark that "there have been no well head failures recorded by industry. It is deemed highly unlikely that any accident failure of a well head would occur." However, during special operations in oil- or gas-filled caverns, eruptions can result from failure of the sealing-off equipment. From the perspective of risk analysis, it is important to evaluate the volume of fluids that would be released from the cavern upon total decompression.

If ρ_h is the density of a stored liquid hydrocarbon and ρ_b the brine density and if the brine at the well-head is submitted to atmospheric pressure, then the hydrocarbon pressure at the well-head is a linear function of the interface depth H_i:

$$P_h = (\rho_b - \rho_h)gH_i \tag{22}$$

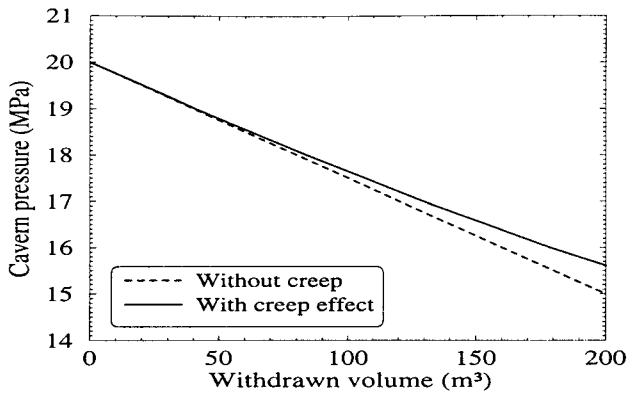

Fig. 11. Transient creep effect during a cavern depressurization.

After failure of the well-head (see Fig. 12), hydrocarbon pressure will drop to zero and the brine level in the central tube will fall to a depth, η, such that the weight of the two fluid columns balance:

$$\rho_b(H_i - \eta) = \rho_h H_i \tag{23}$$

The pressure drop is $P_h = \rho_b g\eta$ and the percentage volume of fluid expelled from the cavern is mainly due to fluid decompression in the cavern:

$$V_{exp}/V = [\beta + x(\beta_h - \beta_b^{ad})](\rho_b - \rho_h)gH_i \tag{24}$$

where β is the compressibility factor and $\beta = \beta_c + \beta_b^{ad}$.

For oil-filled storage ($x \approx 1$) in a 1000 m deep cavern, the relative volume of expelled oil following well-head failure would be 2.7×10^{-3} (or 1350 m^3 for an oil-filled 500,000 m^3 cavern). For propane storage in a 600 m deep cavern, the relative volume of propane expelled would be 1.5×10^{-2} (or 750 m^3 for a propane-filled 50,000 m^3 cavern) (Fig. 13).

2.6.2. Long-term behavior of an abandoned cavern

Due to increasing concern in environmental protection, several projects involving hazardous-waste disposal and cavern abandonment in salt caverns (Tomasko et al. [18], Bérest and Brouard [14]) have motivated several recent papers and studies (Wallner and Paar [19], Behrendt et al. [20]).

For such purposes as hazardous-waste disposal, salt caverns will probably be filled with brine and sealed before being abandoned. If brine thermal expansion and percolation can be disregarded (a somewhat unrealistic hypothesis, see Bérest and Brouard [14], but one which allows simple estimations), pressure will slowly increase in a closed cavern due to creep. For the sake of simplicity, we assume that steady-state creep is reached at any instant. The steady-state volume loss rate due to creep can be written as

$$\dot{V}_{creep}/V = -B(T_a)(P_R - P_c)^n \tag{25}$$

where $B(T_a)$ is a function of rock temperature and P_R is the lithostatic pressure at cavern depth.

Combination with the compressibility relation, $\dot{V}_{creep}/V = -\beta\dot{P}_c$, leads to a differential equation whose integration is straightforward:

$$P_R - P_c(t) = [P_R - P_c(0)]\{1 + (n-1)B[P_R - P_c(0)]^{n-1}t/\beta\}^{(1/1-n)} \tag{26}$$

It must be noted here that the "long-term" compressibility factor, β, is larger than the above mentioned "slow" compressibility factor β^{sat}, due to transient

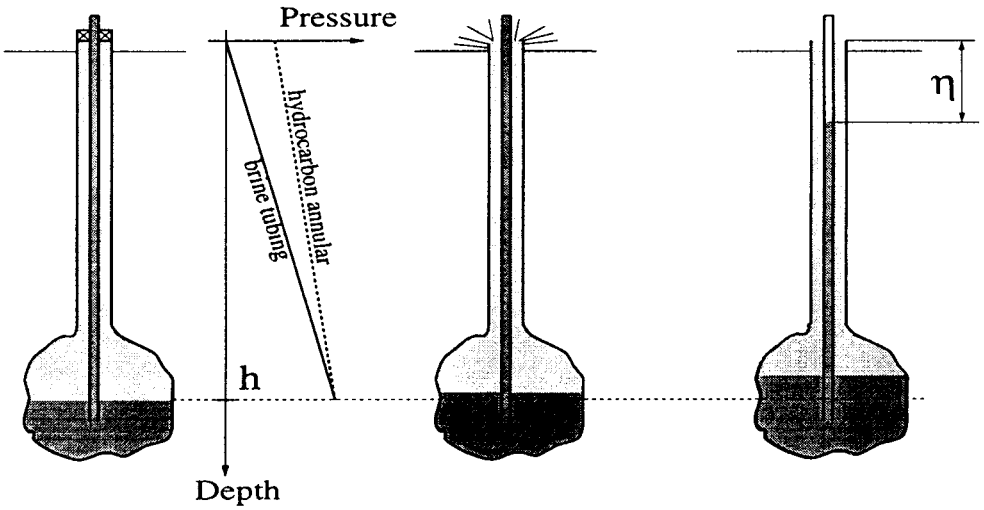

Fig. 12. Blow-out movie.

creep, and includes the effects of brine compressibility, rock compressibility, additional dissolution and transient creep; the last effect is difficult to assess. Typical values for a 1000 m-deep cavern are $n = 3$ and $B = 2.5 \times 10^{-7}$ MPa^{-3} yr^{-1}; the initial difference between lithostatic and brine pressures is $P_R - P_c(0) =$ 10 MPa. How pressure build-up rate is influenced by compressibility factor β is shown on Fig. 14: the standard case is $\beta = 4 \times 10^{-4}$ MPa^{-1} or more; the case of a flat-shaped cavern is given by $\beta = 10^{-3}$ MPa^{-1} and the case of a cavern in which a gas bubble is trapped is given by $\beta = 5 \times 10^{-3}$ MPa^{-1}.

3. Dynamic behavior

3.1. Introduction

In the previous section, we have seen that the fluid(s) contained in an underground cavern and access well, in addition to the cavern and the casing or strings, are elastic bodies. This means that when the fluid(s), the cavern or the well are affected by small changes in pressure or shape, these bodies vibrate according to their mechanical properties, sizes, shapes and their mechanical interactions. These vibrations constitute a source of information that is rarely used, even when the cost of this information is minimal. All that is needed is to record the development of the fluid pressure at the well head.

Holzhausen and Gooch [21], for instance, have analyzed the effects of hydraulic fracture growth on the period of the free vibrations in a closed well; a very similar method has been applied to the same problem by Bérest [22]. Hsu [23] had derived a theoretical relation between the oscillation period and the radius of a penny-shaped fracture.

For a cased well opening into a salt cavern, Bérest et al. [24] have shown that, when a cavern well is opened to the atmosphere, long period waves take place in response to a small pressure drop in the cavern. These waves can be easily measured, which

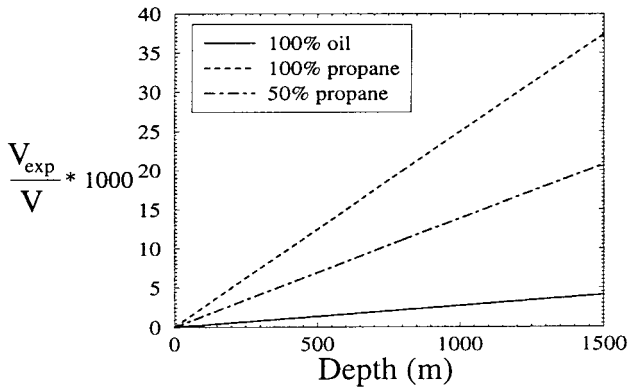

Fig. 13. Relative product volume expelled during a blow-out, as a function of cavern depth.

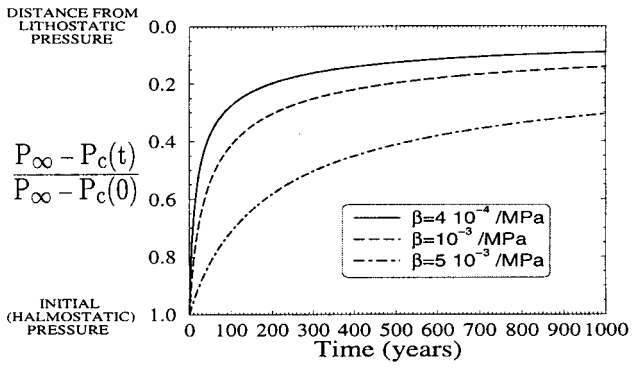

Fig. 14. Cavern pressure build-up rate influenced by compressibility factor β.

allows evaluation of the cavern volume through simple calculations.

In this section, we will consider several types of acoustic waves that can be measured easily. Their relations with salt-cavern properties will be discussed and typical examples will be presented.

3.2. Tubing waves

The first type of wave observed in salt caverns is a well wave, whose period is of the order of one to few seconds. When a rapid change in pressure and/or fluid flow rate takes place in a fluid-filled tube (for instance, when a valve is suddenly closed or opened), this change generates an acoustic wave that travels in the fluid along the well. If the tube were perfectly stiff, the wave celerity would be given by the simple formula

$$\beta_f^{ad}\rho_f c_f^2 = 1 \tag{27}$$

where c_f is the acoustic wave celerity in the fluid, β_f^{ad} is the fluid isotropic compressibility factor and ρ_f is the fluid density. With standard temperature and pressure, typical values of the wave celerity are: $c_w = 1500$ m/s for soft water, $c_a = 340$ m/s for air and $c_b = 1800$ m/s for saturated brine. In fact, the steel tube is also a compressible body; its compressibility factor, β_t, can theoretically be calculated if the characteristics of the tube and its environment (cement, rock mass) are perfectly known, which will hardly be the case. Anyway the global well compressibility factor, $\beta = \beta_t + \beta_f^{ad}$, is larger than β_f^{ad}, resulting in a speed of sound, c, in the well that is smaller than the fluid wave speed:

$$1/c^2 = 1/c_f^2 + \rho_f\beta_t \tag{28}$$

A typical value for water or brine in a tube will be $c = 1000$ m s^{-1}, which means that if, for instance, brine injection in a well is interrupted by the rapid closure of a surface valve, the generated wave will reach a point located 1 km below ground level in one second.

In this example, if the tube cross-section were $S = 250$ cm^2 ($7''^{5/8}$ in diameter) and the brine flow rate before closing the valve were $Q = 90$ m^3 h^{-1}, the fluid speed would be $u = Q/S = 1$ m s^{-1}; the pressure increase behind the travelling down wave due to the sudden valve closure would be $\Delta P = \rho_f c u$ or, in our case if fluid is brine, $\Delta P = 1.2$ MPa (205 psi). Such a phenomenon is called a "water-hammer"; the rapid pressure change shakes and rattles the tube in the well.

The tube shoe opens in so large a cavity (when compared to the very small volume of brine displaced by the wave itself) that, when the wave reaches the tube end, it is not able to modify the pressure in the cavity by any noticeable amount. Then a second wave, traveling upward and transporting a negative pressure change ($-\Delta P = -\rho_b c u$) is generated such that the pressure change, which had been generated by the primary downward wave, vanishes to zero below the upward wave. This wave reaches the well head and in its turn generates a downward wave. After a short time, theses waves combine to form a simple stationary wave; pressure changes or fluid-flow rate variations have the same phase along the entire tube. These stationary waves are dampened, the highest frequency components rapidly vanish, leaving a sinusoidal wave whose period is fixed by the boundary conditions at the top and bottom of the well. Pressure is constant at bottom, as noted above. Flow vanishes to zero at the top if the well head is closed, leading to a so-called "quarter-wave" vibration whose period is $cT = 4H$, H being the tube length. If the well is opened to atmospheric pressure, one theoretically gets a "half wave" ($cT = 2H$); however, because the wave path through the well head is hardly straight, a quarter-wave can often be observed even in the case of an opened well. Such waves can very easily be observed in underground salt caverns provided that an appropriate pressure recording device is set at the well-head. Two examples are given below. Such waves will also be observed when analyzing much longer period waves.

- The first test (Fig. 15) was performed in July 1995 on the Carresse SPR3 cavern. The observed vibrations were triggered by venting of the cavern, during which the well-head pressure suddenly dropped from 0.4 MPa to zero. The oscillation period was $T = 2.5$ s (data acquisition frequency was 20 Hz, as in all tests described below, except for the 1982 Etrez 53 test), which means that $c = 4H/T = 4 \times 692/2.5 \approx 1100$ m s^{-1}.
- The second test (Fig. 16; Fig. 20 displays another test of the same series) was performed in February 1995 on the Etrez 53 cavern, as part of the full test program described by Bérest et al. [7]. The cavern volume was $V \approx 7500$ m^3; the 930 m long central tube was filled with brine; a 140 m high column of nitrogen was lowered into the annular space (Fig.

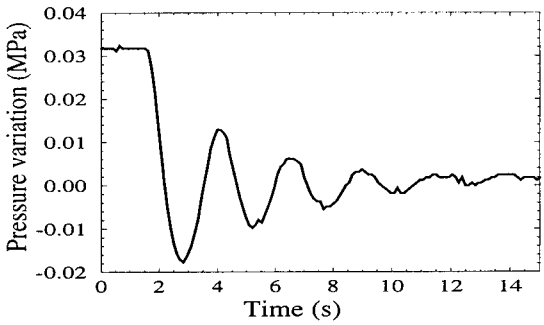

Fig. 15. Quarter-waves in the tubing during the July 1995 Carresse test (Elf Aquitaine).

19). In Fig. 16, long period (20 s) oscillations are clearly observed; they will be discussed later. Half-waves in the nitrogen column ($c = 345$ m s^{-1}, $h =$ 140m) are clearly visible for instance between $t = 60$ s and $t = 70$ s; their periods are $T \approx 0.81$ s or $T = 2h/c$. Quarter-waves in the central brine-filled tube are also clearly visible (for example, between $t = 90$ s and $t = 150$ s; their period is approximately 2.6 s). The brine in the central well is mechanically coupled through the steel-tube to the brine in the annular space and the quarter-wave period is probably slightly modified by this coupling.

3.3. The Helmholtz resonator

In the last paragraph, we considered waves generated by small displacements of the fluid contained in the tube and traveling through the well. An oscillatory phenomenon of another kind intervenes when the well-head is not closed; then large volumes of fluid can be exchanged between the well and the cavity itself, whose pressure now will not be considered as constant. The interface between the liquid and the air, whose seat will be in the well head or inside a container above the well head (Fig. 17), will experience movements of long period (one to several minutes).

3.3.1. Well opened into a large container

Consider, first, a simple example consisting of a cavern and a well filled with brine and opened to the atmosphere in a container whose cross-section (Σ) can be much larger than the cross-section of the tube (S), see Fig. 17.

As seen before, both brine in the cavern and the cavern itself behave as springs, in the sense that both are compressible: a $\dot{P}_c$ pressure-variation rate in the cavern leads to a brine outflow rate through the cavern top, Q, such that:

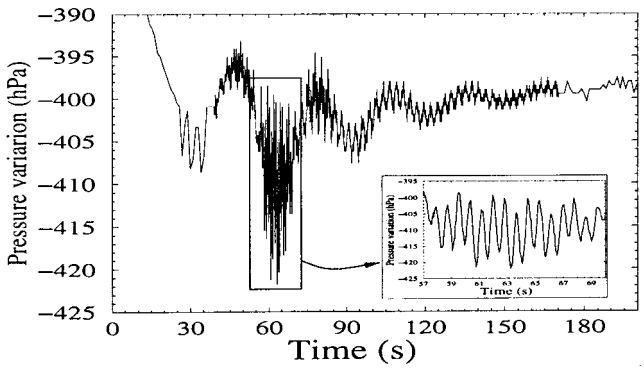

Fig. 16. The February 1995 Etrez test (Gaz de France): Half-waves in the annular space (scroll), quarter-waves in the tubing superposed with a longer period resonator wave.

$$(\beta_c + \beta_b^{ad}) V \dot{P}_c + Q = 0 \tag{29}$$

where V is the cavern volume, β_c and β_b^{ad} are the cavern and brine adiabatic compressibility factors, respectively. The "dynamic" compressibility factor ($\beta = \beta_c + \beta_b^{ad}$) is slightly smaller than its static counterpart, but $\beta = 4 \times 10^{-4}$ MPa^{-1} still appears a reasonable value.

The "stiffness" of a brine-filled (or "lower-spring") cavern (i.e. the ratio between brine flow and the pressure build-up rate), is the inverse of the cavern compressibility:

$$\Delta P / \Delta V_{inj} = 1/[(\beta_c + \beta_b^{ad}) V] \tag{30}$$

For a 100,000 m^3 cavern, this ratio is 2.5×10^{-2} MPa m^{-3}; in other words, it is necessary to force a 40 m^3 volume of brine into the cavern to increase its pressure by 1 MPa.

The volume of brine contained in the central tube will appear, by comparison, as an extremely stiff body. The brine-plus-steel-tube compressibility factor may be not very different from the brine-plus-cavern compressibility factor, but the tube volume is smaller by 3 or 4 orders of magnitude than the cavern volume, resulting in much larger global stiffness ($1/\beta V$). As a whole, the brine in the tube can be considered as a rigid body (In fact, tube waves due to brine compressibility in the tube, which had been described above, do exist, but they do not interfere, due to their much shorter period) whose mass is $\mu = \rho_b SH$, where H is the tube length ($H = 1000$ m is typical), S is the tube cross-section ($S = 25$ lm^{-1} is typical) and ρ_b is the brine density ($\rho_b \approx 1200$ kg m^{-3}). In this example, the tube volume is 25 m^3 and the brine mass is $\mu = 30{,}000$ kg.

The brine in the container at ground level also behaves as a "spring" in the following sense: if a brine flow, Q (in m^3 s^{-1}), is expelled from the cavern, it will

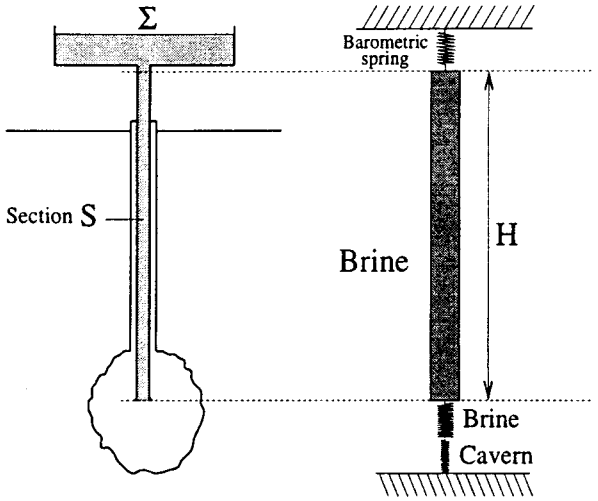

Fig. 17. A salt cavern considered as a mass and spring set.

result in a Q/Σ uprise of the air/brine interface at the well head which, in turn, determines a pressure build-up at the bottom of the container:

$$\dot{P}_2 = \rho_b g Q/\Sigma \tag{31}$$

The barometric stiffness due to gravity forces, or the ratio between the expelled brine flow and pressure build-up in the cavern, in the case of a $\Sigma = 1$ m^2 container cross-section, is

$$\rho_b g/\Sigma = 10^{-2} \text{ MPa m}^{-3} \tag{32}$$

This stiffness is larger when the container cross-section is small. For example, if there is no container and the air/brine interface is located inside the tube itself, the barometric stiffness due to gravity forces will be $\rho_b g/S = 40 \times 10^{-2}$ MPa m^{-3}. In this case, the "upper string" would be much stiffer than the "lower string" constituted by the cavern.

A very large harmonic oscillator — The differential equation satisfied by flow-rate Q is simply reached by considering that brine in the tube, with mass $\mu = \rho_b SH$ and acceleration $\tilde{a} = \dot{Q}/S$, is pushed upward by the cavern pressure excess P_c (excess, when compared to static pressure distribution at rest) and pushed downward by the pressure excess at the bottom of the container P_2, both pressures acting through the tube cross-section:

$$(\rho_b SH)(\ddot{Q}/S) = S(\dot{P}_c - \dot{P}_2) \tag{33}$$

Some straightforward algebra allows elimination of $\dot{P}_c$ and $\dot{P}_2$:

$$\ddot{Q} + \left\{ \frac{S}{\rho_b H(\beta_c + \beta_b^{ad})V} + \frac{gS}{\Sigma H} \right\} Q = 0 \tag{34}$$

The solution of such a differential equation is a sine function, whose period is

$$T = \frac{2\pi}{\omega_o}, \quad \omega_o^2 = \frac{S}{\rho_b H(\beta_c + \beta_b^{ad})V} + \frac{gS}{\Sigma H} \tag{35}$$

The following two limit cases can be examined.

1. The cavern volume is very large and there is no container (the air/brine interface is located in the well). Then, $S = \Sigma$ and the oscillations period is governed by the upper spring stiffness:

$$T = 2\pi\sqrt{H/g} \tag{36}$$

In other words, the system behaves as a simple pendulum, the length of which is equal to the brine column height. A typical period, for $H = 1000$ m and $g = 10$ m s^{-2}, is $T \approx 63$ s.

The cavern volume, V, is small (10,000 m^3, for instance) and the container cross-section, Σ, is very large (several m^2); thus, $(gS/\Sigma H)$ is negligible when compared to the first term, $S/(\rho_b H\beta V)$. In other words, the cavern is a much stiffer spring than the air/brine interface. In such a case, the period of oscillation is in the range of one to two minutes (see example below):

$$T = 2\pi\sqrt{\frac{\rho_b H(\beta_c + \beta_b^{ad})V}{S}} \tag{37}$$

The test was performed in July 1982 on the Etrez 53 cavern. The cavern volume was $V \approx 7500$ m^{-3}, the tube length, H, was 930 m and the tube cross-section, S, was 250 cm^2 (Fig. 18). Data acquisition frequency was 7 Hz. At the beginning of the test, the main valve was closed and brine was forced into the cavern through a pump to increase the cavern pressure. Then the main valve was opened and a long period oscillation ($T =$ 74 s) took place; this was measured through the pressure variations in the fuel-filled annular space. This figure was consistent with the computed value, which was $T \approx 73$ s.

3.3.2. A cavern containing two different fluids

We have considered above the case of several fluids in a cavern; the overall cavern compressibility factor is $\beta = \beta_c + (1 - x)\beta_b^{ad} + x\beta_h^{ad}$ (we consider the adiabatic values), where x is the cavern volume fraction occupied by the other fluid. When applied to vibrations of the cavern, this formula means that the period of the oscillations will vary with fraction x. Let T_{min} be the period of oscillation when there is (for instance) no propane in the cavern (in other words, when the cavern is filled with brine, or $x = 0$). Then the period is given by

$$T = T_{min}\sqrt{\frac{\beta}{\beta_c + \beta_b^{ad}}} = T_{min}\sqrt{1 + x\frac{\beta_h^{ad} - \beta_b^{ad}}{\beta_c + \beta_b^{ad}}} \tag{38}$$

which means that the period will be multiplied by 3

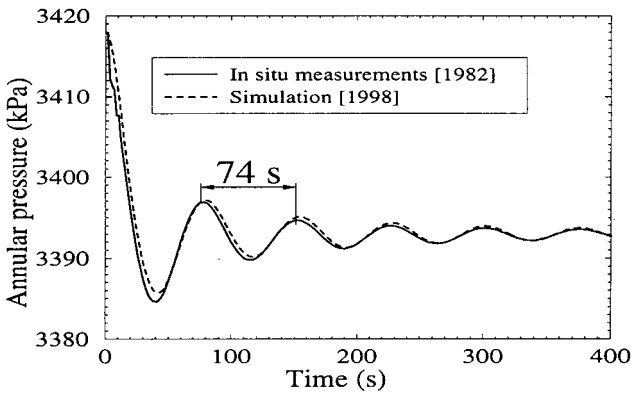

Fig. 18. The 1982 Etrez Test (Gaz de France).

when, for example, the cavern contains 80% propane. Several attempts have been made for applying the former method to the determination of the brine volume/hydrocarbon volume ratio in an underground storage cavern (A "static" method, tested on the Carresse SPR1 cavern, has been described above, Section 2.4.4). Such information is very important; after many injection-withdrawal movements, the exact volume of stored products is not well known. A method of estimation of the volume, based on a simple measurement of natural vibrations period, would have proved useful. Unfortunately, the attempts did not prove to be successful. The reason is that the previous analysis failed to take into account head losses.

3.3.3. Head losses

Head losses are due to the viscosity of brine flowing through the tube, the well head and the flexible tubes at ground level. They bring some dampening (Fig. 18) of the oscillations which, in some cases, become very difficult to record.

We assume first that brine flow rate in the tube is slow enough for the flow to be laminar; then the head losses can be computed according to the classical Poiseuille formula (in other words, we assume that head losses are linearly proportional to flow rate):

$$\ddot{Q} + 2\lambda\dot{Q} + \omega_o^2 Q = 0, \quad \lambda = (4\nu_b\pi)/S \tag{39}$$

where ν_b is the kinematic viscosity of brine ($\nu_b \approx 1.4 \times 10^{-6}$ m^2 s^{-1} for brine at a temperature of 20°C) and S is the tube cross-section. To prevent overdamp, λ must be significantly smaller than ω_o, or $S^3/(\beta V H) \gg 3.8 \times 10^{-7}$ m^2 MPa, a condition that was met during the 1982 Etrez test ($S = 2.5 \times 10^{-2}$ m^2, $\beta V \approx 3$ m^3 MPa^{-1}) but difficult to meet if the cavern is large and compressible or if the tube cross-section is small, as in the SPR3 test described below. The approximation holds for a laminar flow, whose Reynolds number is small enough, typically $\mathsf{R} = 2Q/(\nu_b\sqrt{\pi S}) < 2000$. Because the maximum flow satisfies $Q_{max} = \beta V \omega_o \Delta P_{max}$, pressure variations and then the initial drop must be small (much smaller than 0.1 MPa, as an order of magnitude).

In fact, this formula applies for a clean smooth tube, which a brine tube in a deep well is definitely not. A more realistic law for head losses per unit of length (in Pa m^{-1}) is $\Gamma\,\mathrm{sgn}(Q)\dot{Q}^{1.8}$ with Q in m^3 s^{-1} and

$$\Gamma = 0.154\rho_b^{1.046}\nu_b^{0.196}d^{-4.65} \tag{40}$$

where d is tube internal diameter (m). Then we get the differential equation:

$$\ddot{Q} + \Gamma\,\mathrm{sgn}(Q)|\dot{Q}|^{1.8} + \omega_o^2 Q = 0 \tag{41}$$

whose solution accurately fits the data in the case of the Etrez test (Fig. 18).

3.4. Effect of a gas column in the well

Tightness is an essential issue for underground hydrocarbon storage. Rock salt has an extremely low permeability (A typical range is 10^{-22}–10^{-19} m^2.), but the cemented steel casing can become leaky, usually in old wells. It is important that the mechanical integrity of the well be checked from time to time. A common method used to verify integrity is the so-called nitrogen leak method: a nitrogen column is forced into the brine-filled annular space down under the casing shoe. The nitrogen/brine interface position is located through a logging device and monitored for one to several days. Too large of an interface rise is deemed to be an evidence of a gas leak. Such a system — a brine-filled cavern linked to a gas-filled annular space closed at the well head — is the seat of oscillations of the gas/brine interface and can also be considered as an Helmoltz resonator. The study of these oscillations allows to back-calculate the interface location but, conversely, they can blur the exact location of the interface, making its measurement by a logging tool difficult.

Let h be the equilibrium interface depth and $H_a - h$ is the brine-column height in the annular space (Fig. 19). As long as the oscillations are relatively rapid, the gas pressurizations/depressurizations can be considered to be adiabatic — i.e. absolute gas pressure (P_g) and gas column height h, are related by the adiabatic relation $P_g h^\gamma = \text{constant}$, where γ is the adiabatic constant. In other words,

$$\dot{P}_g = -\gamma P_g \dot{h}/h = \gamma P_g Q/(\tilde{S}h) \tag{42}$$

where $\tilde{S}$ is the annular cross-section. The gas column

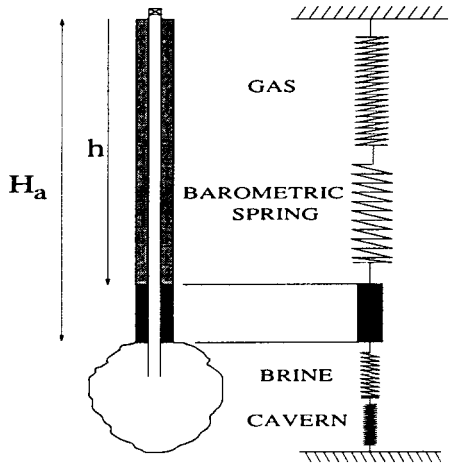

Fig. 19. Mass and spring system for the case of a gas-filled annular space.

stiffness can be roughly evaluated as follows: if $\tilde{S} = 1.4 \times 10^{-2}\ m^2$, $h = 500$ m, $\gamma = 1.4$ and $P_g = 8$ MPa, then the stiffness is $\dot{P}_g/Q = 1.6$ MPa m^{-3}. The "upper spring" now consists of the barometric spring, described above, plus the compressible gas column which also behaves as a spring (Fig. 19):

$$\dot{P}_2 = \rho_b g Q/\tilde{S} + \gamma P_g Q/(\tilde{S}h) \tag{43}$$

These are generally much stiffer than the "lower spring" constituted by the cavern itself. The annular space length is H_a and the differential equation satisfied by brine flow is

$$[\rho_b \tilde{S}(H_a - h)](\ddot{Q}/\tilde{S}) + \left[\rho_b g + \frac{\gamma P_g}{h} + \frac{\tilde{S}}{\beta V}\right] Q = 0 \tag{44}$$

or

$$T = \frac{2\pi}{\omega_o}$$
$$\omega_o^2 = \frac{g}{H_a - h} + \frac{\tilde{S}}{\rho_b (H_a - h)\beta V} + \frac{\gamma P_g}{\rho_b h (H_a - h)} \tag{45}$$

The period clearly depends upon gas-column height and vanishes when the gas column is either very long ($h = H_a$) or very short ($h = 0$) (However, see Section 3.5). The gas pressure variations, as measured in the annular space and the brine pressure variations, as measured in the central tube, are, respectively:

$$\dot{P}_{ann} = \frac{P_g \gamma}{\tilde{S}h} Q \quad \text{and} \quad \dot{P}_{tub} = -\frac{Q}{\beta V} \tag{46}$$

In some cases, their amplitudes can be notably different, with opposite signs.

As seen on Fig. 20, the oscillations triggered by a brine venting on the central tube can clearly be observed on the annular space. The cavern is Etrez 53, the tube length is $H = 930$ m and the gas column in the annular space is 200 m high. The absolute gas pressure was $P_g = 7$ MPa. For nitrogen, $\gamma = 1.4$; furthermore, $\tilde{S} = 14.7\ l\ m^{-1}$ then $T \approx 20$ s. This oscillation is not clearly visible in the tube, as can be expected from the low $\dot{P}_{tub}/\dot{P}_{ann} \approx 0.05$ ratio. Shorter vibrations whose periods is 2.6 s can also be observed both in the tube and the annular space; they probably are quarter-waves, which are coupled through the steel tubes (note that the phases are opposite) and maybe through the cavern itself.

3.5. Gas pocket trapped in the well head

The SPR3 cavern, with its abnormally high compressibility due to a gas pocket trapped in the cavern, has been described previously (Section 2.4.5). The well head was equipped with a pressure gauge whose resolution was 250 Pa; the data acquisition period was 0.05 s. The initial objective of the first test, called test 0, was to observe Helmholtz-resonator oscillations in the opened cavern, as had been made during the 1982 Etrez test. After build up of a small pressure excess in the closed cavern, opening of a well-head valve (which takes place 300 s after test start on Fig. 21) vents the cavern and triggers short-period stationary quarter-waves, followed by a longer period oscillation. The period, assuming a tube cross-section $S = 81$ cm^2, should have been 145 s (see equation above); but dampening appear to be high (due to small tube cross-section) and the oscillation rapidly vanishes (Fig. 21).

Much clearer, but totally unexpected, oscillations are triggered in the closed cavern when the injection pump stops, 100 s after test start. These oscillations are *anharmonic*: crests are spiky and troughs are rounded, resulting in uncommon asymmetric pressure-versus-time curves. This effect dwindles and the so-called "period" becomes smaller when signal amplitude is dampened with time. These facts are best shown on a further test in which initial amplitude was larger (Fig. 22); the pressure origin is the same as in Fig. 21. During a second series of tests (Fig. 23), numbered from 1 to 7, 700 l of brine were injected in 100 l steps, again triggering anharmonic vibrations whose "periods" are significantly reduced (from 15 to 8 s for

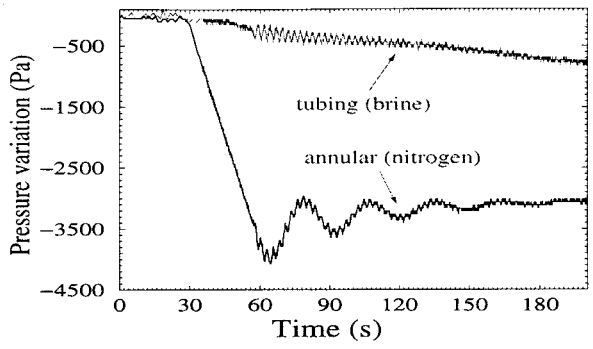

Fig. 20. Brine venting during the February 1995 Etrez test.

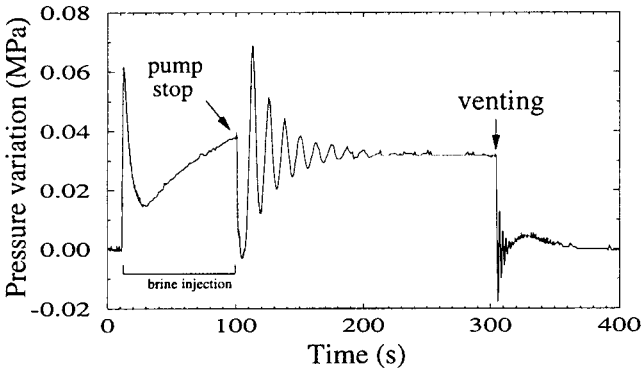

Fig. 21. The July 1995 test on SPR3 cavern (Elf Aquitaine).

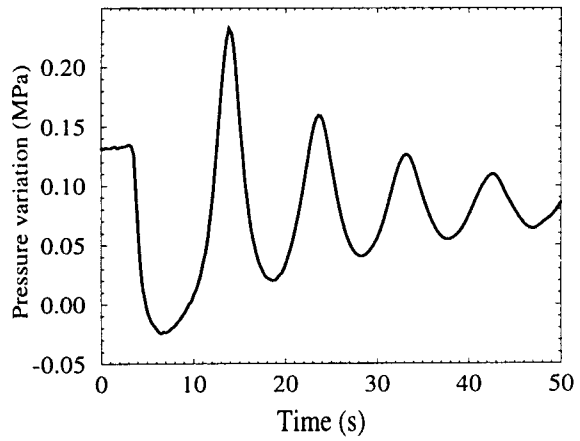

Fig. 22. Anharmonic oscillations during the July 1995 tests.

the period measured just after pump stops) when the well head pressure increases following each brine injection. Only the existence of a very compressible nonlinear elastic body included in the (cavern plus well) system can be responsible for these unexpected features. The gas pocket trapped in the cavern is not a good candidate: its high pressure (8.3 MPa) makes it a relatively stiff body. A better hypothesis appears to be the existence of a small amount of gas (a few liters) trapped at the well head in the annular space. Its pressure is close to atmospheric; then even small brine-gas interface displacements can drastically modify the gas volume and generate nonlinear pressure build-up. If P and h are the gas-column (absolute) pressure and height, respectively, the adiabatic gas compression can be described as above:

$$Ph^{\gamma} = P_1 h_1^{\gamma} \tag{47}$$

(Sub 1 refers to the figures when the cavern is at rest.) The cavern is compressible, as outlined above; displacement of the gas/brine interface from h_1 to h forces a volume, $\tilde{S}(h-h_1)$, into the cavern ($\tilde{S}$ is the annular cross-section area), that builds up the cavern pressure by

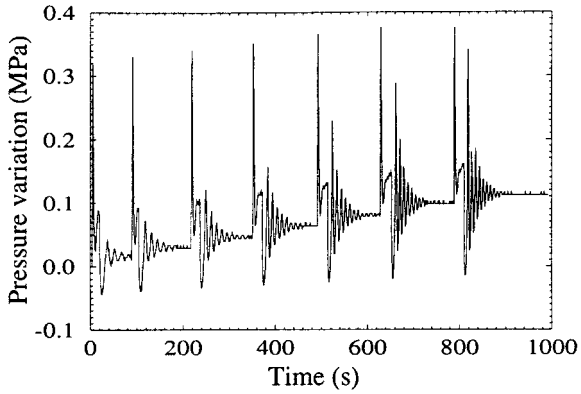

Fig. 23. Pressure oscillations during brine injections.

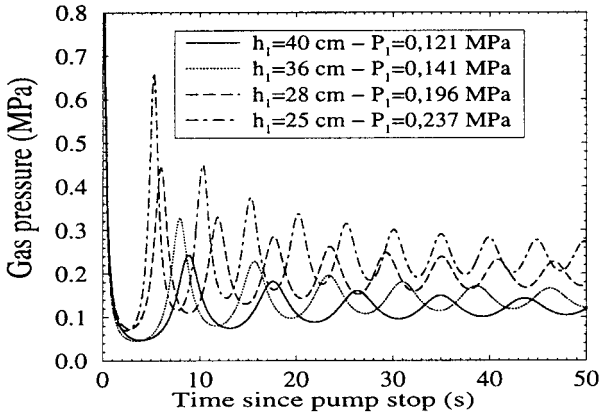

Fig. 24. Numerical simulation of anharmonic oscillations.

$$\beta V(p-p_1) = \tilde{S}(h-h_1) \tag{48}$$

Then the momentum equation for the brine column in the annular space can be written:

$$(H_a - h)(\rho_b \ddot{h} + \bar{\omega}) = P - P_1 - \rho_b g(h-h_1) - (p-p_1) \tag{49}$$

where $\bar{\omega}$ are head losses (in Pa m^{-1}); typically, $\bar{\omega} = \mathrm{sgn}(\dot{h})\kappa|\dot{h}|^{1.85}$, where $\kappa = 1.35 \times 10^6$ I.S. units. Some straightforward algebra leads to a nonlinear differential equation that allows back-calculation of the gas column height (Fig. 24): the best-fit sets the brine/gas interface 170 cm below the brine/air interface during test 0, which means that the gas pressure was $P_1 = 0.121$ MPa. Period of the movement as a function of the kinetic energy is drawn on Fig. 25 for different values of the average gas pressure. The agreement with the data shown in Fig. 23 is satisfactory. After the test, the annular space was opened to the atmosphere and gas flew out of the well head.

3.6. Closed cavern, tube and annular space gas-filled

In this case, both the annular space (cross-section $\tilde{S}$

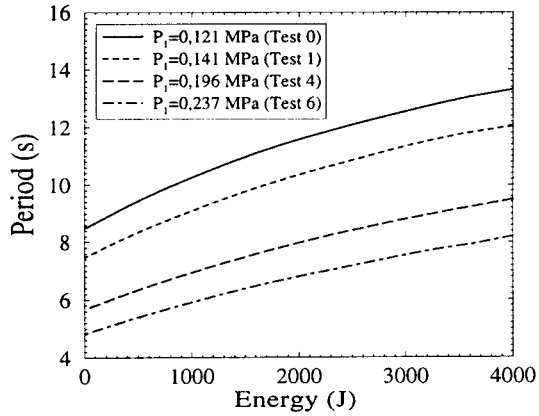

Fig. 25. Evolution of oscillation period with kinetic energy.

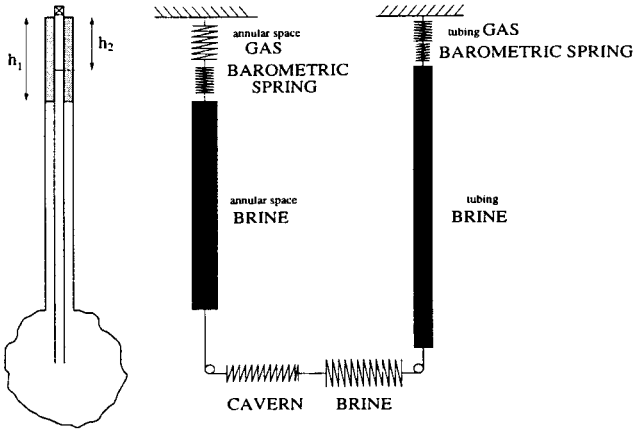

Fig. 26. Gas in the annular space and in the tube.

and length H_a) and central tube (cross-section S and length H) contain some gas (Fig. 26). The whole system consists of two masses (The brine masses that are contained in the annular space, $\mu = \rho_b \tilde{S}(H_a - h_1)$ and in the central tube, $\mu' = \rho_b S(H - h_2)$, respectively) whose oscillations are coupled through a set of elastic springs:

$$\begin{cases} (\rho_b \tilde{S}(H_a - h_1))(\ddot{Q}_1/\tilde{S}) = \tilde{S}(\dot{P} - \gamma P_g^1 Q_1/(\tilde{S}h_1) + \rho_b g Q_1/\tilde{S}) \\ (\rho_b S(H - h_2))(\ddot{Q}_2/S) = S(\dot{P} - \gamma P_g^2 Q_2/(Sh_2) + \rho_b g Q_2/S) \\ \beta V \dot{P} + (Q_1 + Q_2) = 0 \end{cases} \tag{50}$$

The initial (or static) gas pressures, P_g^1 and P_g^2, are linked by

$$P = P_g^2 + \rho_b g(H - h_2) = P_g^1 + \rho_b g(H - h_1) \tag{51}$$

The system is characterized by two distinct periods. The real pressure variations are a certain combination of two basic oscillations (eigenmodes):

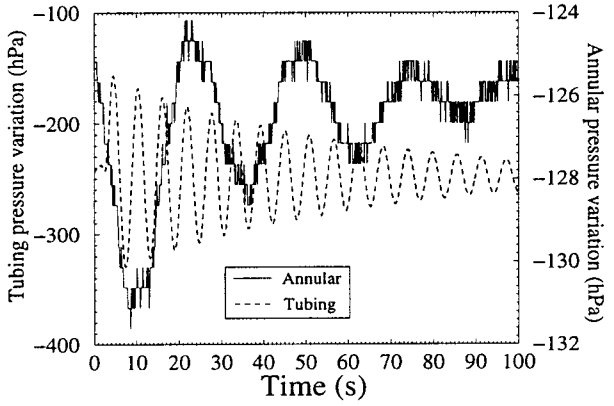

Fig. 27. The February 1996 Etrez MIT Test (Gaz de France).

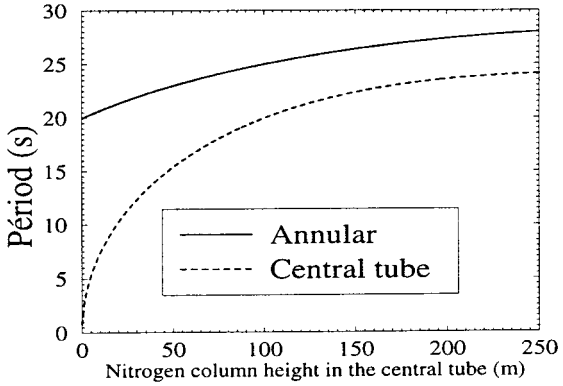

Fig. 28. Evolution of the two distinct periods.

$$\begin{bmatrix} \frac{\mu'}{\tilde{S}} & 0 \\ 0 & \frac{\mu}{S} \end{bmatrix} \begin{bmatrix} \ddot{Q}_1 \\ \ddot{Q}_2 \end{bmatrix} + \begin{bmatrix} \frac{\mu'\omega_1^2}{\tilde{S}} & \frac{1}{\beta V} \\ \frac{1}{\beta V} & \frac{\mu\omega_2^2}{S} \end{bmatrix} \begin{bmatrix} Q_1 \\ Q_2 \end{bmatrix} = [0] \tag{52}$$

where ω_1 et ω_2 are the pulsations when there is no link between the tube and the annular space (i.e. when setting $1/(\beta V) = 0$).

The test (Fig. 27) was performed on the Etrez 53 cavern. A nitrogen column was lowered approximately 400 m below ground level in the annular space. Unexpectedly, the tube became leaky and some gas entered the central tube. Pressure variations at the well head were recorded during venting of the tube gas. The gas/brine interface is much higher in the central tube and its oscillation period much shorter. On Fig. 28 are displayed the periods measured in the tubing and in the annular space as a function of the gas-brine interface depth in the central tube (which was unknown but appears to be small).

4. Conclusions

Much useful information can be inferred from recording the pressure oscillations that are triggered when brine injection or withdrawal stops — for instance, the volume of a salt cavern, the LPG-volume/brine-volume ratio in a LPG storage cavern and the existence of small gas pockets trapped in the well head. A further advantage is that information can be obtained for relatively *little cost*.

Acknowledgements

The authors have benefited from comments by Gerard Durup and Michel Pottier, of the Gaz de France Company and Florian Lehner, visiting professor at Ecole Polytechnique. They are indebted to the staffs of

the Etrez (GDF), Carresse (ELF) and Manosque (GEOSTOCK) storage sites, also to Yves Le Bras and Vincent De Greef from Ecole Polytechnique, who provided valuable assistance in performing the tests. Special thanks to Kathleen Sikora.

References

[1] Hardy RH, Langer M. Proc. 1st Conf. Mech. Beh. Salt. Clausthal-Zellerfeld: Trans. Tech. Pub, 1984 [901 pp.].
[2] Hardy RH, Langer M. Proc. 2nd Conf. Mech. Beh. Salt. Clausthal-Zellerfeld: Trans. Tech. Pub, 1988 [781 pp.].
[3] Hardy RH, Langer M, Bérest P, Ghoreychi M. Proc. 3rd Conf. Mech. Beh. Salt. Clausthal-Zellerfeld: Trans. Tech. Pub, 1996 [621 pp.].
[4] Aubertin M, Hardy RH. Proc. 4th Conf. Mech. Beh. Salt. Clausthal-Zellerfeld: Trans. Tech. Pub, 1998 [658 pp.].
[5] Hugout B. Mechanical behavior of salt cavities — in situ tests — model for calculating the cavity volume evolution. In: 2nd Conf. Mech. Beh. Salt. Clausthal-Zellerfeld: Trans. Tech. Pub, 1988. p. 291–310.
[6] Ehgartner BL, Linn JK. Mechanical behavior of sealed SPR caverns. S.M.R.I. Fall Meeting, Houston, 1994.
[7] Bérest P, Bergues J, Brouard B, Durup G, Guerber B. A tentative evaluation of the M.I.T. S.M.R.I. Spring Meeting, Houston, 1996.
[8] Thiel WR. Precision methods for testing the integrity of solution mined underground storage caverns. In: Proc 7th Symp on Salt, Vol. I. Amsterdam: Elsevier, 1993. p. 671–82.
[9] Boucly P. In-situ tests and behaviour modelisation of salt cavities for storage of natural gas. Rev Fr Geotechnique 1982;18:49–58 [in French].
[10] Colin P, You T. Salt geomechanics seen through 20 years experience at the Manosque Facility. S.M.R.I. Spring Meeting, Paris, 1990.
[11] You T, Maisons C, Valette M. Experimental procedure for the closure of the brine production caverns on the "Saline de Vauvert" Site. S.M.R.I. Fall Meeting, Hannover, 1994.
[12] Brouard B. On the behavior of solution-mined caverns, theorical study and in situ experimentation. PhD Thesis, Ecole Polytechnique Palaiseau France, 1998 [in French].
[13] Crotogino FR. Salt cavern in-situ testing from the constructor's and the operator's view point. In: Proc. 1st Conf. Mech. Beh. of Salt. Clausthal-Zellerfeld: Trans. Tech. Pub, 1984. p. 613–28.
[14] Bérest P, Brouard B. Behavior of sealed solution-mined caverns. S.M.R.I. Spring Meeting, New-Orleans, 1995.
[15] Istvan JA, Evans LJ, Weber JH. Rock mechanics for gas storage in bedded salt caverns. Proc 36th US Rock Mech Symp, Int J Rock Mech Min Geo Abstr 1997;34:647.
[16] Clerc-Renaud A, Dubois D. Long term operation of underground storage in salt. In: Proc 5th Symp on Salt, Vol II. Cleveland: Norther Ohio Geol. Society, 1966. p. 3–12.
[17] Van Fossan NE, Whelpy FV. Nitrogen as a testing medium for proving the mechanical integrity of wells, S.M.R.I. Fall Meeting, Houston, 1985.
[18] Tomasko D, Elcock D, Veil J, Caudle D. Risk Analyses for Disposing Nonhazardous Oil Field Wastes in Salt Caverns. In: Argonne National Laboratory Report. US Department of Energy, Office of Fossil Energy, 1997 [Contract W-31-109-ENG-38].
[19] Wallner M, Paar WA. Risk of progressive pressure build up in a sealed cavity, S.M.R.I. Fall Meeting, El Paso, 1997.
[20] Behrendt C, Crotogino FR, Hackney J. S.M.R.I.-Bibliography for Cavern Abandonment, 1997.
[21] Holzhausen GR, Gooch RP. The effect of hydraulic-fracture growth on free oscillations of wellbore pressure. In: Proc. 26th US Rock Mech. Symp., Rapid City, 1985. p. 621–5.
[22] Bérest P. Vibratory phenomena in oil drill holes. Application to the calculation of the volume of underground cavities. Rev Fr Geotechnique 1985;32:5–17 [in French].
[23] Hsu YC. Forced oscillations of the Los Alamos Scientific Laboratory's Dry Hot Rock Geothermal Reservoir. Report LA-6170-MS, Los Alamos Scientific Laboratories, 1975.
[24] Bérest P, Habib P, Boucher M, Pernette E. Periodic flow of brine in the drilling hole of a salt cavern, Application to the determination of its volume. In: Proc. 24th US Rock Mech. Symp., 1983. p. 813–8.